Gas-Phase Interaction of H_2S with O_2: A Kinetic and Quantum Chemistry Study of the Potential Energy Surface

Alejandro Montoya,* Karina Sendt, and Brian S. Haynes

Department of Chemical Engineering, The University of Sydney, Sydney, NSW 2006, Australia

Received: May 16, 2004; In Final Form: September 30, 2004

Quantum chemical calculations were carried out to study the interaction of hydrogen sulfide with molecular oxygen in the gas phase. The basic mechanism, the rates of reaction, and the potential energy surface were calculated. Isomers and transition states that connect the reactants with intermediates and products of reaction were identified using the G2 method and B3LYP/6-311+G(3df,2p) functional. Hydrogen abstraction to form HO_2 + SH is the dominant product channel and proceeds through a loose transition state well-described at the level of calculation employed. The temperature dependence of the rate coefficient in the range 300–3000 K has been determined on the basis of the ab initio potential energy surface and with variational transition-state theory. The reaction is 169.5 kJ mol^{-1} endothermic at 0 K with a rate constant given by $2.77 \times 10^5\,T^{2.76}\exp(-19\,222/T)$ $cm^3\,mol^{-1}\,s^{-1}$ and should proceed slowly under atmospheric thermal conditions, but it offers a route to the initiation of H_2S combustion at relatively low temperatures.

Introduction

The reactions of H_2S in combustion have received relatively little attention because, in general practice, the conversion of H_2S to SO_2 is rapid and essentially complete. Early work on the development of detailed chemical mechanisms for the reactions of H_2S and other sulfur species[1−3] has not been developed to a comprehensive extent, as is apparent from recent reviews.[4,5] Although recent work on the reactions of SO_2 in combustion environments has enhanced our understanding of how this species is converted to SO_3, promotes the recombination of radical species, and interacts with NO_x chemistry,[6−8] the fact remains that the reactions of H_2S and the mechanism of SO_2 formation remain unclear. This gap is of particular significance to combustion under fuel-rich and non-premixed conditions, to gasification processes, and especially to the front-end furnace of the industrially important Claus process (in which H_2S is partially combusted in O_2 to form SO_2 and elemental sulfur). While we have recently developed and validated a comprehensive mechanism for the thermolysis of H_2S,[9] it remains to understand the interaction of oxygen with this system.

Experimental and ab initio studies have been devoted to the analysis of the thermodynamics and kinetics of H_2S with oxygen atoms and hydroxyl radicals, because of their importance in atmospheric chemistry, and the mechanism and rates of these processes have been established.[10−12] In contrast, the reaction of H_2S with O_2, which is likely to be an initiation step in H_2S combustion[3] and possibly important also under slow thermal oxidation conditions, has remained unstudied. Several ab initio studies have analyzed the stability of some neutral $[H_2,S,O_2]$ structures that could be produced from the reaction of H_2S with O_2,[13−17] but there are very few experimental studies of such species.[18−20] The only isomer that has been clearly identified experimentally and theoretically is HOSOH,[19] which has been rationalized as one of the most stable $[H_2,S,O_2]$ isomers[15,16] in the gas phase, although no detailed analysis of the potential energy surface of H_2S/O_2 has been published. Therefore, the aim of the present paper is to provide thermodynamics, kinetics, and spectroscopic information on sulfur species involved in the reaction of H_2S with O_2.

Methodology

The strategy consists of a series of ab initio and density functional quantum chemical calculations of a number of hydrogen–sulfur–oxygen species. These calculations are used to examine the potential energy surface and the kinetics of the reaction of H_2S with molecular oxygen. The geometry of reactants, transition states, and possible products of reactions are fully optimized using the full second-order Moller–Plesset many-body perturbation theory and B3LYP functional using the 6-31G(d) and 6-311+G(3df,2p) basis sets, respectively. Spin-restricted wavefunctions are used for all closed-shell species and spin-unrestricted functions for all open-shell species. A normal-mode analysis is performed on each stationary point to characterize it either as a minimum (all vibrational frequencies real) or as a transition state (a single imaginary frequency). The reactants and products connected by each transition state are confirmed by following the minimum energy paths using the Gonzalez–Schlegel IRC algorithm[21] in both directions at the optimized level. The energy of the MP2(full)/6-31G(d) optimized structures is refined using the G2 and G3 methodologies,[22,23] where the MP2(full)/6-31G(d) zero-point vibrational energy (ZPE) is used instead of the HF/6-31G(d) ZPE. The resulting frequencies and ZPEs at the MP2(full)/6-31G(d) level are scaled by a factor of 0.9427 to take account of inadequacies at this level.[24] Electronic structure calculations are carried out using the *Gaussian 03* program.[25] Temperature-dependent rate constants are calculated using the variational transition-state theory based on the minimum energy reaction pathway. The reaction pathway is followed in steps of 0.005 bohr at the desired quantum chemistry level. Determinations of the rate constants are calculated using the *Virtual Kinetic Laboratory*.[26]

* Corresponding author. E-mail: montoya@chem.eng.usyd.edu.au.

10.1021/jp047903p CCC: $30.25
Published on Web 01/21/2005

TABLE 1: Comparison of Predicted Heat of Reaction (kJ mol^{-1}) with that Calculated from the Literature

reaction	MP2(full)/ 6-31G(d) ΔH_r (0 K)	B3LYP/ 6-311+G(3df,2p) ΔH_r (0 K)	G2 ΔH_r (0 K)	G3 ΔH_r (0 K)	literature ΔH_r (0 K)
$H_2S + O_2 \Leftrightarrow HO_2 + SH$	+210.7	+170.1	+169.5	+170.3	+176.5
$H_2S + O_2 \Leftrightarrow HSO + OH$	+120.7	+38.3	+33.2	+29.9	+29.4
$H_2S + O_2 \Leftrightarrow SO + H_2O$	−178.9	−201.5	−216.0	−218.2	−216.3
$H_2S + O_2 \Leftrightarrow SO_2 + H_2$	−244.6	−234.4	−270.3	−268.6	−276.7

Results

Heats of Reactions. Products of reaction on the potential energy surface of H_2S/O_2 that were analyzed are shown below:

$$H_2S + O_2 \Leftrightarrow HO_2 + SH \tag{1}$$

$$H_2S + O_2 \Leftrightarrow HSO + OH \tag{2}$$

$$H_2S + O_2 \Leftrightarrow SO + H_2O \tag{3}$$

$$H_2S + O_2 \Leftrightarrow SO_2 + H_2 \tag{4}$$

The calculated enthalpies of reaction at 0 K using the MP2(full)/6-31G(d), B3LYP/6-311+G(3df,2p), G2, and G3 levels of theory are summarized in Table 1 together with literature data. The theoretical heats of reaction were obtained as the differences in our calculated total energies of the reactants and products at 0 K. The literature heats of reaction are based on the heats of formation obtained from the JANAF tables,[27] except for those species where more accurate heats of formation have been recently reported, such as the case for OH (ΔH_f(0 K) = 37.0 kJ mol^{-1}),[28] SH (ΔH_f(0 K) = 143.2 kJ mol^{-1}),[29] HO_2 (ΔH_f(0 K) = 13.4 kJ mol^{-1}),[30] and HSO. The heat of formation of HSO has been the subject of considerable uncertainty, with various high-level computational results consistently showing lower values (∼−20 kJ mol^{-1}) than crossed molecular beam studies (−3.8 kJ mol^{-1}).[31] More recent experimental work[32] has shown that earlier experimental results may have failed to account adequately for the product internal energy, so the computational results are probably more reliable. High-level quantum chemistry calculations have been carried out on the heat of formation of HSO. Xantheas and Dunning have been able to correctly predict the relative stability of HSO and SOH using multireference ab initio methods with a sequence of correlation-consistent basis sets.[33,34] A heat of formation of ΔH_f(0 K) = −22.6 ± 5.4 kJ mol^{-1} at the complete basis-set limit was reported.[33] A recent multireference ab initio study has found that including tight d functions in the basis set improves the convergence of the predicted energies with respect to the basis-set size.[35] Denis and Ventura have shown that DFT methods also correctly predict the relative stability of HSO and SOH, and the heats of formation of both species converged rapidly with an increase in the basis-set size.[36] Here, we take the value reported by Denis and Ventura of ΔH_f(0 K) = −24.9 kJ mol^{-1} for HSO.[36]

All of the methods employed predict endothermic heats of reaction for the product channels 1−2 and exothermic heats of reaction for product channels 3−4 in accordance with the heats of reaction calculated using literature data. The errors in predicting the heats of reaction using the MP2(full)/6-31G(d) energies are decreased by using the G2 and G3 methodologies. Notice that G2 and G3 energies are computed at the optimized geometry using the MP2(full)/6-31G(d) level, so the improvement in accuracy for the predicted values of heat of reaction is due to a better description of the electron correlation and increased basis-set size. G2 predicts heats of reaction within ±7.5 kJ mol^{-1} of the literature data, and no systematic improvement is achieved by calculating the heat of reaction using the G3 method. The differences in the predicted heats of reaction using the G2 and G3 methods are within 3.3 kJ mol^{-1}. The best method to predict heats of formation of sulfur species is still under debate, because the estimated values are sensitive to the electron−electron interaction and basis sets.[37] This is evident in comparing the G2 and G3 heats of reaction with the B3LYP/6-311+G(3df,2p) level of theory. The B3LYP density functional has been found to give very precise enthalpy of formation values of several species related to HSO.[36] The results presented in Table 1 for several $H_2S + O_2$ reactions support this finding. However, the G2 results are in generally closer agreement with the literature data for the studied reactions. The heats of reaction to form $SO + H_2O$ and $SO_2 + H_2$ using the B3LYP/6-311+G(3df,2p) level of theory are underestimated by 14.8 and 42.3 kJ mol^{-1}, respectively, relative to the literature data, apparently because of bad predictions of the heats of formation of SO_2 and SO. On the basis of the heats of reaction calculated for the products of reactions 1−4, it is expected that stable species on the potential energy surface of H_2S/O_2 can be described adequately using the G2 methodology.

Isomers of the Neutral H_2SO_2. The present results show that seven isomers of the form [H_2,S,O_2] may be formed after the interaction of O_2 with H_2S. The structures are sketched in Figure 1 together with some optimized parameters. All of the isomers were found to be minima on the potential energy surface with a singlet ground state. The absolute G2 total energies and the MP2(full)/6-31G(d) scaled vibrational frequencies of the respective isomers are summarized in Table 2.

It is found that the most stable isomer is the sulfoxylic acid, in agreement with other studies.[15,16] Two rotamers of the

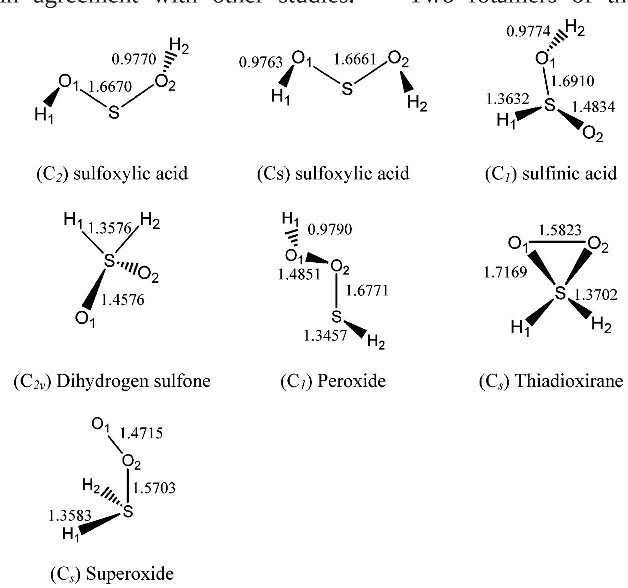

Figure 1. Isomers of the form [H_2,S,O_2] on the potential energy surface of $H_2S + O_2$. Some geometrical parameters computed using the MP2(full)/6-31G(d) level of theory are shown in the figure. Bond lengths are given in angstroms, and symmetry is shown in parentheses. The complete geometry is given as Supporting Information.

TABLE 2: Total Energies (in au) and Scaled Vibrational Frequencies (in cm^{-1}) of the Optimized Intermediates in the $H_2S + O_2$ Reaction

	G2 energy	MP2(full)/6-31G(d) vibrational frequency
C_2 sulfoxylic acid	−549.178188	313, 508, 519, 759, 768, 1181, 1185, 3494, 3497
C_s sulfoxylic acid	−549.176337	324, 451, 546, 761, 767, 1164, 1183, 3498, 3500
sulfinic acid	−549.168867	320, 403, 698, 959, 1086, 1170, 1205, 2413, 3511
dihydrogen sulfone	−549.154585	462, 860, 960, 1104, 1200, 1288, 1363, 2465, 2486
peroxide	−549.088553	205, 338, 392, 700, 752, 971, 1282, 2584, 3485
thiadioxirane	−549.004655	57, 663, 683, 856, 1008, 1068, 1377, 2361, 2389
superoxide	−549.002398	290, 319, 721, 820, 838, 965, 1230, 2458, 2480

sulfoxylic acid in C_2 and C_s symmetries have been identified, as shown in Figure 1 where the C_2 sulfoxylic acid is 4.9 kJ mol^{-1} more stable than the C_s rotamer. Frank et al.[19] analyzed the stability of the C_2 and C_s sulfoxylic rotamers using the G2 method and predicted that the C_2 isomer is more stable by 5 kJ mol^{-1}, in agreement with our results. Sulfoxylic acid is the most stable isomer, followed by sulfinic acid, dihydrogen sulfone, peroxide, thiadioxirane, and superoxide, which are 24.5, 62.0, 235.4, 455.6, and 461.6 kJ mol^{-1}, respectively, above the C_2 sulfoxylic acid energy at 0 K. The two least stable isomers, the thiadioxirane and the superoxide, are unlikely to be observable experimentally in the gas phase because they are unstable with respect to dissociation to $H_2S + O_2$ in the singlet spin state, with estimated heats of reaction for dissociation of $\Delta H_r = -84.8$ and -90.8 kJ mol^{-1}, respectively. The sulfoxylic acid in C_2 symmetry is also the most stable [H_2,S,O_2] isomer at the B3LYP/6-311+G(3df,2p) level, followed by the C_s sulfoxylic acid, sulfinic acid, dihydrogen sulfone, peroxide, thiadioxirane, and superoxide, which are 4.9, 21.5, 63.6, 230.7, 437.8, and 451.4 kJ mol^{-1}, respectively, above the C_2 sulfoxylic acid energy at 0 K. The relative stabilities of the stable isomers at the two levels of theory are similar, with the unstable thiadioxirane and superoxide isomers predicted to be more stable by 17.8 and 10.2 kJ mol^{-1} at the B3LYP/6-311+G(3df,2p) level. The energy difference between the stable [H_2,S,O_2] isomers calculated using the G2 method and the B3LYP6-311+G(3df,2p) level of theory are within ±4.7 kJ mol^{-1}. Our calculated relative stability of the stable isomers differs from those reported using the MP4/6-31G(d)//MP2/3-21G(d)[15] and MP4(full)/6-31G(d)//MP2/6-31G(d)[16] levels of theory. The energy difference at the MP4 levels is predicted to be two times higher than our calculated values. The energy predicted at the G2 method is believed to be more accurate, because the electron−electron correlation is better described.

Reaction Path Properties. Pathways that connect the [H_2,S,O_2] isomers with the reactants and products of the reactions 1−4 are shown in Figure 2. The figure shows the potential energy surface of the ground state based on the G2 method at 0 K. The energies and the scaled vibrational frequencies of the transition states are summarized in Table 3. The calculated potential energy surface shows the lowest energy paths of the $H_2S + O_2$ interaction. The energy values are relative to the ($^1H_2S + {}^3O_2$) reactant energy.

Initial interaction of H_2S with O_2 may lead to three different reaction channels: the direct evolution of HO_2 + SH and the formation of two stable isomers, the peroxide and the sulfinic acid, which can then decompose to other reaction products as

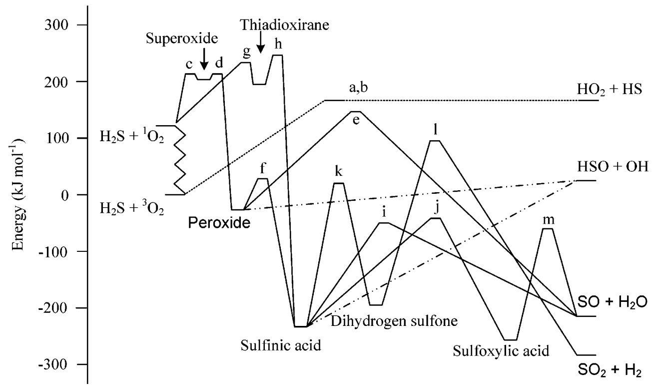

Figure 2. G2 schematic energy profile of the $H_2S + O_2$ reaction. The energies are relative to the $H_2S + {}^3O_2$ reactant energies. Letters on the figure represent the transition-state structures schematized in Figure 3. Dotted lines represent channels of reaction with loose transition states.

shown in Figure 2. Direct hydrogen abstraction from H_2S according to reaction 1 to form HO_2 + SH has an energy barrier similar to the endothermicity of reaction ($\Delta H = +169.5$ kJ mol^{-1}) and is similarly described at the G2 and B3LYP/6-311+G(3df,2p) levels. The transition state ($H_2S/O_2 \rightarrow HO_2$ + HS) is found to be on the spin-triplet surface. Two rotamers of the transition state were identified, and they are shown in Figure 3a and b. Although a small barrier exists at the MP2(full)/6-31G(d) level of theory, the G2 energies of the triplet transition states lie 0.7 and 0.5 kJ mol^{-1} below the energy of the products and 168.8 and 169.3 kJ mol^{-1} above the energy of the triplet reactant energy, suggesting that there is effectively no energy barrier for the reverse reaction. Frenklach et al.[3] proposed that this reaction is the chief initiation step in H_2S oxidation. Under propagating reaction conditions, the reverse process becomes important as a chain termination step.[3]

Transition states formed after oxygen interaction with the sulfur atom are calculated to be in the spin-singlet ground state. The triplet interaction is repulsive, while the singlet interaction is attractive. The triplet reactant energy ($H_2S + {}^3O_2$) is 112.5 kJ mol^{-1} more stable than the spin-singlet reactant energy ($H_2S + {}^1O_2$), as schematized in Figure 2. However, as the oxygen approaches the sulfur atom at a distance of 2.0 Å, the energy of the singlet spin state structure becomes 15.8 kJ mol^{-1} more stable than the triplet spin state structure. The mixing of the singlet−triplet spin states may occur before the formation of the singlet transition states, which occurs at a distance of ∼1.7 Å as shown in Figure 3c and d. A triplet−singlet crossing during H_2S-O_2 interaction may occur with no induced energy barrier.

As shown in Figure 2, formation of peroxide involves the formation of the unstable superoxide intermediate and two transition states ($H_2S + O_2 \rightarrow$ superoxide and superoxide $\rightarrow$ peroxide). The optimized geometrical details of the transition states for these two steps are shown in Figure 3c and d, and the G2 energies and MP2(full)6-31G(d) scaled vibrational frequencies are given in Table 3. The energies of the two transition states and of the superoxide intermediate are very similar. Transition states c and d are 5.0 and 2.3 kJ mol^{-1} above the superoxide structure, respectively. Therefore, the lifetime of the superoxide intermediate in the gas phase should be extremely short. Decomposition of peroxide to reaction products HSO + OH, with no reverse barrier, and transformation to sulfinic acid have the lowest energy barriers, 52.3 and 56.2 kJ mol^{-1}, respectively. As shown in Figure 2, formation of SO + H_2O from the peroxide is a possible reaction channel but with a high

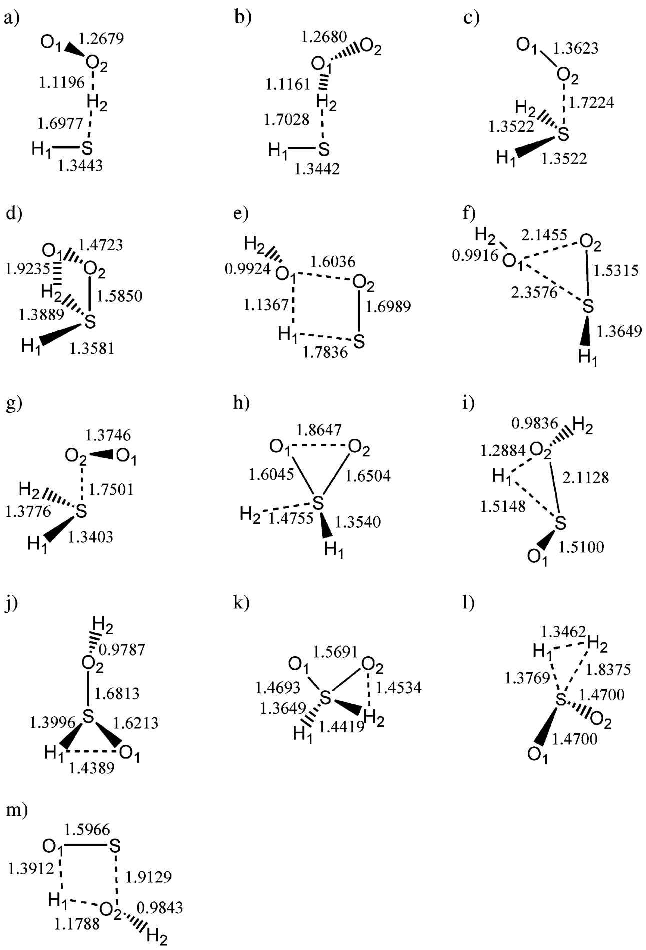

Figure 3. Geometrical representation of the various transition states for the $H_2S + O_2$ reaction. Some geometrical parameters computed on the ground state using the MP2(full)/6-31G(d) level of theory are shown in the figure. Bond lengths are given in angstroms. The complete optimized geometry is given as Supporting Information.

TABLE 3: Total Energies (in au) and Scaled Vibrational Frequencies (in cm^{-1}) of the Transition States in the $H_2S + O_2$ Reaction[a]

TS	G2 energy	MP2(full)/6-31G(d) vibrational frequencies
a	−549.015539	2899*i*, 24, 158, 366, 435, 771, 1292, 1476, 2616
b	−549.015343	2770*i*, 50, 133, 380, 458, 541, 1398, 1476, 2617
c	−549.000466	731*i*, 302, 336, 683, 891, 939, 1197, 2505, 2512
d	−549.001524	599*i*, 361, 588, 829, 877, 944, 1227, 2225, 2475
e	−549.020567	1580*i*, 281, 408, 594, 772, 962, 1308, 1572, 3352
f	−549.068633	168*i*, 137, 352, 384, 782, 988, 1032, 2426, 3332
g	−548.990646	834*i*, 256, 375, 795, 921, 992, 1141, 2341, 2607
h	−548.988067	1018*i*, 507, 723, 905, 977, 1079, 1154, 1787, 2505
i	−549.096291	1600*i*, 222, 377, 444, 784, 1090, 1224,1782, 3445
j	−549.094390	1706*i*, 308, 393, 660, 720, 960, 1132, 2407, 3487
k	−549.075582	1462*i*, 369, 611, 954, 1043, 1121, 1222, 2175, 2378
l	−549.043983	1974*i*, 43, 621, 661, 982, 985, 1079, 1315, 2347
m	−549.104853	1565*i*, 408, 471, 663, 869, 937, 1345,1805, 3448

[a] All of the transition states are in the spin-singlet state except (a) and (b), which are in the spin-triplet state. The wavenumber of the imaginary frequency is followed by the letter *i*.

energy barrier, 178.5 kJ mol^{-1}. The two transition states identified (peroxide → SO + H_2O; sulfinic acid) are shown in Figure 3e and f, and the energy and vibrational frequencies are shown in Table 3. Transition state e is formed after a hydrogen migration from the sulfur atom to the OH group, while f is formed upon OH group migration to the sulfur atom.

TABLE 4: Transition-State Parameters for the Hydrogen Abstraction through a Loose Transition State

r(S−H) (Å)	frequencies (cm^{-1})	moments of inertia (au)
1.6464	3863*i*, 95, 223, 417, 451, 828, 1216, 1457, 2611	40.6, 561.0, 594.8
1.6822	3299*i*, 51, 179, 387, 441, 794, 1279, 1462, 2615	40.8, 561.1, 595.1
1.6924	3038*i*, 34, 165, 374, 437, 779, 1289, 1471, 2615	40.9, 561.1, 595.2
1.6977	2899*i*, 24, 158, 366, 435, 771, 1292, 1476, 2616	40.9, 561.1, 595.2

As shown in Figure 2, the formation of sulfinic acid from $H_2S + O_2$ involves the formation of the unstable thiadioxirane intermediate and two transition states ($H_2S + O_2$ → thiadioxirane and thiadioxirane → sulfinic acid). The geometries of the transition states for these reactions are shown in Figure 3g and h, and the energy and vibrational frequencies are given in Table 3. The energies of the transition states are 234.1 and 240.9 kJ mol^{-1} above the energy of the triplet reactants and 36.8 and 43.6 kJ mol^{-1} above the thiadioxirane isomer energy. No experimental information exists on the relative stability of the thiadioxirane and superoxide isomers, as they have not been detected experimentally. However, using ab initio methods, Shangguan and McAllister[13] predict that thiadioxirane is more stable than the superoxide, although the energy difference nearly vanishes by correcting the energy of the MP2-optimized structure at the QCISD(T)/6-31+G(d) level of theory. The thiadioxirane is predicted to be 6.0 kJ mol^{-1} more stable than the superoxide isomer at the G2 method, showing a small energy difference as suggested by Shangguan and McAllister.[13]

Sulfinic acid can undergo different transformations, as shown in Figure 2. The two lowest energy paths involve the decomposition to SO + H_2O and the transformation to the most stable sulfoxylic acid isomer. Transition states involved in these steps (sulfinic acid → SO + H_2O; sulfoxylic acid) were identified and are shown in Figure 3i and j, and the energy and frequencies are shown in Table 3. The energy barriers for these processes are 190.5 and 194.7 kJ mol^{-1}. Other, higher-barrier channels of reaction from sulfinic acid are the formation of products HSO + OH with $\Delta H = 267.0$ kJ mol^{-1}, with no reverse barrier, and transformation to dihydrogen sulfone through the transition state shown in Figure 3k with an energy barrier of 244.9 kJ mol^{-1}. The backward reaction (sulfinic acid → $H_2S + O_2$) is unlikely to occur because the energy barrier, 474.7 kJ mol^{-1}, is much higher than the energy for the lowest energy path.

The other two stable isomers, dihydrogen sulfone and sulfoxylic acid, can be decomposed to reaction products SO_2 + H_2 and SO + H_2O. The transition states for these processes are shown in Figure 3l (dihydrogen sulfone → $SO_2 + H_2$) and m (C_2 sulfoxylic acid → H_2O + SO). The energies and frequencies are shown in Table 3. The energy barriers for these reactions are 290.4 and 192.6 kJ mol^{-1}, respectively.

Rate Constants. We have calculated thermal rate constant coefficients for the reaction of H_2S with molecular oxygen in the spin-triplet surface to form HO_2 and HS, as this is a dominant pathway because of its low energy barrier. The formation of HO_2 + SH has the lowest energy barrier, and the rate constants were calculated using variational transition-state theory over the 300−3000 K temperature range. The minimum energy potential was followed using the MP2(full)/6-31G(d) level with an energy correction at the stationary points by the G2 method. Tunneling correction was not included in the rate constant as there is no barrier above the endothermicity using either the G2 method or B3LYP/6-311+G(3df,2p) level. The triplet transition state

TABLE 5: Temperature-Dependent Rate Constant Values ($cm^3\ mol^{-1}\ s^{-1}$) for Different Structures in the Reaction Coordinate of Hydrogen Abstraction (reaction 1)

r(S−H) (Å)	temperature (K)					
	300	1000	1500	1600	2500	3000
1.6464	1.24×10^{-14}	5.43×10^{5}	6.75×10^{8}	1.71×10^{9}	3.43×10^{11}	1.90×10^{12}
1.6822	4.90×10^{-16}	2.55×10^{5}	4.53×10^{8}	1.20×10^{9}	3.06×10^{11}	1.82×10^{12}
1.6924	2.90×10^{-16}	2.39×10^{5}	4.52×10^{8}	1.21×10^{9}	3.22×10^{11}	1.94×10^{12}
1.6977	3.13×10^{-16}	2.64×10^{5}	5.03×10^{8}	1.34×10^{9}	3.59×10^{11}	2.17×10^{12}

in cis configuration (Figure 3a) is used to follow the reaction coordinate. Mapping the potential energy surface as the hydrogen atom (H1 in Figure 3a) rotates 180° around the S−H−O axis while keeping other degrees of freedom fixed shows an energy barrier of 0.6 kJ mol^{-1} at the MP2(full)/6-31G(d) level. Therefore, the torsional rotation that interconverts the cis and trans transition states is most effectively treated as a free rotor to recognize the lack of rigidity with respect to this motion. In the computation of the rate constant, the low frequency that interconverts the cis to the trans transition state is replaced by a moment of inertia of 5.88 au to calculate the rate of reaction. The moment of inertia is calculated using the formalism suggested by East and Radom.[38] Rotational symmetry was taken into account by taking a symmetry factor of 2 for each O_2 and H_2S, giving a total symmetry factor of 4.

The MP2(full)/6-31G(d) scaled vibrational frequencies and the moments of inertia for different stationary points along the reaction coordinate are shown in Table 4. The calculated rate constants at different temperatures for the formation of HO_2 + HS are giving in Table 5. The structure that minimizes the hydrogen abstraction rate constant varies with temperature. The structure that minimizes the hydrogen abstraction rate constant below 1500 K is located at a bond length r(S−H) = 1.6924 Å. At this bond length, the transition state is a product-like structure. Above 1500 K, the minimum of the rate constant is located at a bond length r(S−H) = 1.6822 Å. The difference in energy barrier and structure between these two minimum points is fairly small and shows that the minimum in the rate constant is a product-like structure over the whole temperature range 300−3000 K.

Fitting the calculated minimum rate constant coefficients to the three-parameter Arrhenius-type expression in the temperature range 300−3000 K in steps of 100 K is calculated by a least square minimization procedure and leads to $k = 2.77 \times 10^5\ T^{2.76} \exp(-19\,222/T)$ $cm^3\ mol^{-1}\ s^{-1}$ for the $H_2S + O_2 \rightarrow HS + HO_2$ reaction. As no previous rate constants have been published for this reaction, we are not able to make a comparison with the literature. However, Frenklach et al.[3] suggest a value of 1×10^{12} $cm^3\ mol^{-1}\ s^{-1}$ for the reverse reaction. This value is significantly lower than our value of the reverse constant at 1000 K of 7.75×10^{13}, although it must be recognized that the overall mechanism employed in Frenklach et al.[3] is very crude.

Conclusion

The reaction of $H_2S + O_2$ in the ground state has been characterized by quantum chemistry methods. The heats of reaction for different product channels were calculated. While the reactions of hydrogen sulfide with molecular oxygen to form HSO + OH and SH + HO_2 are endothermic processes, the reactions to form $SO_2 + H_2$ and SO + H_2O are exothermic. Several isomers and transition states of the form [H_2,S,O_2] have been identified on the potential energy surface that connects the products of reaction with the reactants. The relative stabilities of the isomers are in the following order: sulfoxylic acid > sulfinic acid > dihydrogen sulfone > peroxide > thiadioxirane > superoxide. Hydrogen abstraction from H_2S by O_2 to form SH + HO_2 is a dominant channel of reaction with a variational transition-state theory rate constant given by $k(T) = 2.77 \times 10^5\ T^{2.76} \exp(-19\,222/T)$ $cm^3\ mol^{-1}\ s^{-1}$.

Acknowledgment. The authors acknowledge the support of the Australian Research Council and the Australian Partnership for Advanced Computing.

Supporting Information Available: Tables with the optimized geometries of the reactants, products, isomers, and transition states on the H_2S-O_2 potential energy surface. This material is available free of charge via the Internet at http://pubs.acs.org.

References and Notes

(1) Muller, C. H., III; Schofield, K.; Steinberg, M.; Broida, H. P. *Proc. Combust. Inst.* **1979**, *17*, 867.
(2) Bernez-Cambot, J.; VoVelle, C.; Delbourgo, R. *Proc. Combust. Inst.* **1981**, *18*, 777.
(3) Frenklach, M.; Lee, J. H.; White, J. N.; Gardiner, W. C. J. *Combust. Flame* **1981**, *41*, 1.
(4) *Kinetics and Mechanism of the Oxidation of Gaseous Sulfur Compounds*; Hynes, A. J., Wine, P. H., Eds.; Springer: New York, 2000; p 343.
(5) Schofield, K. *Combust. Flame* **2001**, *124*, 137.
(6) Alzueta, M. U.; Bilbao, R.; Glarborg, P. *Combust. Flame* **2001**, *127*, 2234.
(7) Mueller, M. A.; Yetter, R. A.; Dryer, F. L. *Int. J. Chem. Kinet.* **2000**, *32*, 317.
(8) Hughes, K. J.; Tomlin, A. S.; Dupont, V. A.; Pourkashanian, M. *Faraday Discuss.* **2001**, *119*, 337.
(9) Sendt, K.; Jazbec, M.; Haynes, B. S. *Proc. Combust. Inst.* **2003**, *29*, 2439.
(10) Goumri, A.; Rocha, J.-D. R.; Laakso, D.; Smith, C. E.; Marshall, P. *J. Chem. Phys.* **1994**, *101*, 9405.
(11) Goumri, A.; Rocha, J.-D. R.; Laakso, D.; Smith, C. E.; Marshall, P. *J. Chem. Phys.* **1995**, *102*, 161.
(12) Goumri, A.; Laakso, D.; Rocha, J.-D. R.; Smith, C. E.; Marshall, P. *J. Chem. Phys.* **1995**, *102*, 161.
(13) Shangguan, C.; McAllister, M. A. *THEOCHEM* **1998**, *422*, 123.
(14) Otto, A. H.; Steudel, R. *Eur. J. Inorg. Chem.* **2000**, 617.
(15) Laakso, D.; Marshall, P. *J. Phys. Chem.* **1992**, *96*, 2471.
(16) Steiger, T.; Steudel, R. *THEOCHEM* **1992**, *257*, 313.
(17) Boyd, R. J.; Gupta, A.; Langler, R. F.; Lownie, S. P.; Pincock, J. A. *Can. J. Chem.* **1980**, *58*, 331.
(18) Fender, M. A.; Sayed, Y. M.; Prochaska, F. T. *J. Phys. Chem.* **1991**, *95*, 2811.
(19) Frank, A. J.; Sadilek, M.; Ferrier, J. G.; Turecek, F. *J. Am. Chem. Soc.* **1997**, *119*, 12434.
(20) Frank, A. J.; Sadilek, M.; Ferrier, J. G.; Turecek, F. *J. Am. Chem. Soc.* **1996**, *118*, 11321.
(21) Gonzalez, C.; Schlegel, B. H. *J. Chem. Phys.* **1989**, *90*, 2154.
(22) Curtiss, L. A.; Raghavachari, K.; Trucks, G. W.; Pople, J. A. *J. Chem. Phys.* **1991**, *94*, 7221.
(23) Curtiss, L. A.; Raghavachari, K.; Redfern, C. P.; Rassolov, V.; Pople, J. A. *J. Chem. Phys.* **1998**, *109*, 7764.
(24) Scott, A. P.; Radom, L. *J. Phys. Chem.* **1996**, *100*, 16502.
(25) Frisch, M. J.; Trucks, G. W.; Schlegel, H. B.; Scuseria, G. E.; Robb, M. A.; Cheeseman, J. R.; Montgomery, J. A., Jr.; Vreven, T.; Kudin, K. N.; Burant, J. C.; Millam, J. M.; Iyengar, S. S.; Tomasi, J.; Barone, V.; Mennucci, B.; Cossi, M.; Scalmani, G.; Rega, N.; Petersson, G. A.; Nakatsuji, H.; Hada, M.; Ehara, M.; Toyota, K.; Fukuda, R.; Hasegawa, J.; Ishida, M.; Nakajima, T.; Honda, Y.; Kitao, O.; Nakai, H.; Klene, M.; Li, X.; Knox, J. E.; Hratchian, H. P.; Cross, J. B.; Adamo, C.; Jaramillo, J.;

Gomperts, R.; Stratmann, R. E.; Yazyev, O.; Austin, A. J.; Cammi, R.; Pomelli, C.; Ochterski, J. W.; Ayala, P. Y.; Morokuma, K.; Voth, G. A.; Salvador, P.; Dannenberg, J. J.; Zakrzewski, V. G.; Dapprich, S.; Daniels, A. D.; Strain, M. C.; Farkas, O.; Malick, D. K.; Rabuck, A. D.; Raghavachari, K.; Foresman, J. B.; Ortiz, J. V.; Cui, Q.; Baboul, A. G.; Clifford, S.; Cioslowski, J.; Stefanov, B. B.; Liu, G.; Liashenko, A.; Piskorz, P.; Komaromi, I.; Martin, R. L.; Fox, D. J.; Keith, T.; Al-Laham, M. A.; Peng, C. Y.; Nanayakkara, A.; Challacombe, M.; Gill, P. M. W.; Johnson, B.; Chen, W.; Wong, M. W.; Gonzalez, C.; Pople, J. A. *Gaussian 03*, revision B.05; Gaussian, Inc.: Pittsburgh, PA, 2003.

(26) Zhang, S.; Truong, T. N. *Kinetics module of the CSEO program*; http://www.cseo.net/(2003 released).

(27) Chase, M. W., Jr. *J. Phys. Chem. Ref. Data* **1998**, 1, Monograph 9.

(28) Herbon, J. T.; Hanson, R. K.; Golden, D. M.; Bowman, C. T. *Proc. Combust. Inst.* **2003**, *29*, 1201.

(29) Shiell, R. C.; Hu, X. K.; Hu, Q. J.; Hepburn, J. W. *J. Phys. Chem. A* **2000**, *104*, 4339.

(30) Ramond, T. M.; Blanksby, S. J.; Kato, S.; Bierbaum, V. M.; Davico, G. E.; Schwartz, R. L.; Lineberger, W. C.; Ellison, G. B. *J. Phys. Chem. A* **2002**, *106*, 9641.

(31) Balucani, N.; Casavecchia, P.; Stranges, D.; Volpi, G. G. *Chem. Phys. Lett.* **1993**, *211*, 469.

(32) Quandt, R. W.; Wang, X.; Tsukiyama, K.; Bersohn, R. *Chem. Phys. Lett.* **1997**, *276*, 122.

(33) Xantheas, S. S.; Dunning, T. H. J. *J. Phys. Chem.* **1993**, *97*, 18.

(34) Xantheas, S. S.; Dunning, T. H. J. *J. Phys. Chem.* **1993**, *97*, 6616.

(35) Wilson, A. K.; Dunning, T. H., Jr. *J. Phys. Chem. A* **2004**, *108*, 3129.

(36) Denis, P. A.; Ventura, O. N. *Int. J. Quantum Chem.* **2000**, *80*, 439.

(37) Denis, P. A. *Chem. Phys. Lett.* **2003**, *382*, 65.

(38) East, A. L. L.; Radom, L. *J. Chem. Phys.* **1997**, *106*, 6655.